Effect of Sediment Size Scaling on Physical Modeling of Bridge Pier Scour

Seung Oh Lee[1] and Terry W. Sturm, M.ASCE[2]

Abstract: Local pier scour experiments were performed in the laboratory to investigate the effect of relative sediment size on pier scour depth using three uniform sediment sizes and three bridge pier designs at different geometric model scales. When the data from a large number of experimental and field investigations are filtered according to a Froude number criterion, the effect of relative sediment size on dimensionless pier scour depth is brought into focus. The choice of sediment size in the laboratory model distorts the value of the ratio of pier width to sediment size in comparison with the prototype which in turn causes larger values of scour depth in the laboratory than in the field. This model distortion due to sediment size is shown to be related to the scaling of the large-scale unsteadiness of the horseshoe vortex by studying the relevant time scales of its coherent structure upstream of a bridge pier using acoustic Doppler velocimeter measurements. Observations of sediment movement, probability distributions of velocity components, and phase-averaging of velocity measured upstream of a bridge pier reveal properties of coherent motions that are discussed in terms of their contribution to the relationship between dimensionless pier scour depth and the ratio of pier width to sediment size over a large range of physical scales.

DOI: 10.1061/(ASCE)HY.1943-7900.0000091

CE Database subject headings: Hydraulic models; Scour; Sediment transport; Turbulence; Piers; Bridges.

Introduction

Bridge scour is a significant transportation problem because of the structural damage, economic disruption, and possible loss of life that can occur when it results in bridge foundation failure (Stamey 1996; Parola et al. 1998; Richardson and Davis 2001; Morris and Pagan-Ortiz 1999; Wardhana and Hadipriono 2003). Despite significant research efforts to improve bridge pier scour prediction methods, one of the most vexing problems is the scaling issue of translating pier scour depths measured in the laboratory to prototype scour depths. Nevertheless, several bridge scour prediction formulas have been developed based on experimental studies alone because of the difficulty in modeling analytically or numerically the complex three-dimensional (3D) interaction of the river flow with the obstruction presented by the bridge foundation and with the erodible bed of the river. These experimental studies have focused on empirical correlations of the relevant dimensionless variables to predict the maximum equilibrium value of scour depth, d_s, which is then scaled up to the prototype scale according to the geometric scale ratio (Melville and Sutherland 1988; Melville 1997; Richardson and Davis 2001; Melville and Coleman 2000). When such scaled scour predictions are compared with field observations obtained using the latest in mobile instrumentation techniques by the U.S. Geological Survey (USGS) (Landers and Mueller 1996, Mueller and Wagner 2005), the overall impression is an overprediction of field scour by laboratory formulas, although the field data exhibit a considerable degree of scatter. Whether this data scatter and overprediction of d_s is due to imprecise knowledge of the flow conditions and degree of time development of scour at the time of the measurements or to laboratory scaling issues, or both, remains to be determined.

Laboratory-based pier scour prediction formulas begin from a dimensional analysis of the problem which is used to present the laboratory data in terms of dimensionless variables. A typical dimensional analysis result (Ettema et al. 1998; Sturm 2001) is given by

$$\frac{d_s}{b} = f\left(K_s, K_\theta, \frac{y_1}{b}, \frac{V_1}{V_c}, \frac{b}{d_{50}},\ \mathsf{F}_1 \text{ or } \mathsf{F}_b,\ \mathsf{R}_1 \text{ or } \mathsf{R}_b\right) \tag{1}$$

where b=bridge pier width; K_s=shape factor; K_θ=pier alignment factor; d_{50}=median sediment size; y_1 and V_1=approach flow depth and velocity, respectively; V_c=critical velocity for initiation of sediment motion; F_1=approach flow Froude number $(V_1/\sqrt{gy_1})$; F_b=pier Froude number $(V_1/\sqrt{gb})$; R_1=approach flow Reynolds number $(V_1 y_1/\nu)$; and R_b=pier Reynolds number $(V_1 b/\nu)$. The influences of the first four factors on the right-hand side of Eq. (1) on d_s/b are rather well-known (Melville and Coleman 2000). The pier Reynolds number, R_b, has not usually been considered to have a strong influence on scour depth as long as the flow around the pier is fully-turbulent (Ettema et al. 1998). Furthermore, the mean distance to the separation point at the bed measured upstream of the bridge pier nondimensionalized by b appears to be only weakly dependent on R_b as R_b becomes large based on a literature review of experimental measurements (Lee 2006).

The pier Froude number, F_b, is found to be a significant variable affecting local scour around a bridge pier by Shen et al. (1969). Ettema et al. (1998) suggest that dependence of d_s/b on F_b is not adequately accounted for in leading scour formulas.

[1]Instructor, School of Urban and Civil Engineering, Hongik Univ., Seoul 121-791, South Korea.

[2]Professor, School of Civil and Environmental Engineering, Georgia Institute of Technology, Atlanta, GA 30332 (corresponding author).

Note. This manuscript was submitted on January 24, 2008; approved on April 13, 2009; published online on April 15, 2009. Discussion period open until March 1, 2010; separate discussions must be submitted for individual papers. This paper is part of the ***Journal of Hydraulic Engineering***, Vol. 135, No. 10, October 1, 2009. ©ASCE, ISSN 0733-9429/2009/10-793–802/$25.00.

They explain that F_b reflects the variation of pressure gradients around the pier in a free surface flow. More recently, Ettema et al. (2006) have shown that decreasing F_b or increasing R_b by increasing b while holding all other variables constant results in smaller d_s. They propose that this reduction in d_s is related to lower frequencies of shedding of wake vortices for piers of larger width.

In the field, the effect of sediment size, d_{50}, has not been considered to be important to pier scour because of very large values of b/d_{50} (Breusers and Raudkivi 1991; Raudkivi 1986). In the laboratory, d_s/b tends to increase with b/d_{50} up to a maximum at $b/d_{50} \cong 25$ and seemingly becomes independent of the ratio when b/d_{50} is greater than 50 (Raudkivi 1986). However, Sheppard et al. (2004) have suggested that d_s/b may decrease at very large values of b/d_{50} based on experiments in a large flume. Therefore, the value of b/d_{50} can represent one of the primary differences between field and laboratory results when considering all parameters affecting local scour around a bridge pier.

The laboratory scaling issue is partly attributable to the choice of model sediment size which is related to similarity considerations associated with the values of F_1 and b/d_{50} in model and prototype. Scaling d_{50} according to the geometric scale based on Shields' criterion results in very small model sediment sizes exhibiting interparticle forces that are not present in sand-bed rivers. This has led to the practice of reproducing the flow intensity factor (V_1/V_c) which can violate Froude number similarity because of the larger critical velocities associated with model sediment sizes that are necessarily too large. An additional model distortion occurs with respect to the value of b/d_{50} due to the constrained choice of model sediment size. It is this latter model distortion and its relationship to the large-scale unsteadiness of the horseshoe vortex system that forms upstream of the pier that is the subject of this paper.

Both laboratory and field measurements are employed in this study to investigate the effect of laboratory d_{50} on the scaling of d_s through the influence of the parameter b/d_{50}. In addition, the coherent turbulent structure of the horseshoe vortex system is explored with selected measurements of the unsteady characteristics of the large-scale motion. An explanation for the role of the parameter b/d_{50} is offered in terms of its connection to scaling of the large-scale unsteadiness of the horseshoe vortex.

Experimental Investigation

All experiments on local scour around bridge piers were conducted in the hydraulics laboratory of the School of Civil and Environmental Engineering at the Georgia Institute of Technology, Atlanta, Georgia. River models and flat-bed models were built inside a 4.3 m wide by 24.4 m long horizontal flume and a 1.1 m wide by 24.4 m long rectangular tilting flume, respectively. The maximum water flowrate in the laboratory is 0.3 m^3/s supplied by two centrifugal pumps and a large constant-head tank through a 305 mm diameter supply pipe. Water supply to the flume is recirculated such that water flows into the laboratory sump at the downstream end of the flume from which it is continuously pumped into an overflowing constant-head tank. The flowrate into the flume is controlled by gate valves installed in a 305 mm supply pipe for high flowrates, and in a 152 mm supply pipe for flowrates less than 0.06 m^3/s. Magnetic flow meters are installed in both supply pipes, and they have an expected measurement uncertainty of $\pm 2.8 \times 10^{-4}$ m^3/s.

An instrument carriage is set up on longitudinal steel rails attached by leveling bolts to the walls of the flumes. The carriage can be moved upstream or downstream along the flumes and used to support the velocity meter and point gauge. The point gauge, which is used for measurement of elevations, and the velocity meter are mounted on the carriage and can be positioned accurately in three-dimensions.

Two acoustic Doppler velocimeters (ADVs), with acoustical frequencies of 10 MHz and 16 MHz, were used to measure instantaneous point velocities and turbulence quantities. The ADVs were mounted on a point gauge attached to the steel rail of the instrument carriage. The ADV cylindrical sampling volume, which is located a distance of 5 cm below the probe, has a diameter of 6.0 mm and a height of 7.2 mm for the 10 MHz ADV and a diameter of 4.5 mm with a height of 4.5 mm for the 16 MHz MicroADV (SonTek 2001). The ADV was operated at a frequency of 25 Hz, and the sampling duration was at least 2 min. The water depth and bed elevations before and after scouring were measured by the point gauge and the ADV, respectively. It was determined that the ADV can be used to measure the distance from the center of the sampling volume to a solid boundary with an uncertainty of ± 1 mm.

Voulgaris and Trowbridge (1998) have demonstrated in flume experiments that the ADV can accurately measure both mean velocities and Reynolds stresses. Experimental issues of noise from ADVs caused by regions of high turbulence and proximity to boundaries have been discussed extensively in the literature and remedies have been offered (Goring and Nikora 2002; Garcia et al. 2005). In this study, the time record was filtered according to the protocol described in Ge et al. (2005) such that values of the bed shear stress calculated from measured velocity profiles by the Clauser method agreed within 3% of those obtained from Reynolds stress profiles measured by the ADV. In this filtering protocol, the criterion for rejecting a time record at a given data point location was set at an overall average correlation parameter less than 70%, or equivalently, if less than 50% of the data were retained by filtering individual samples below the 70% correlation value, the entire record for that point location was rejected. Despiking using the phase-space algorithm proposed by Goring and Nikora (2002) was also attempted, but once a given time record was filtered, despiking made a negligible change in the turbulence statistics (Ge et al. 2005). Using the protocol described, measurements of approach flow profiles of longitudinal turbulence intensity and turbulence kinetic energy were shown to agree quite closely with accepted semitheoretical and experimental relationships for rough beds (Ge et al. 2005). In addition, a long time record was divided into 2 min ensembles to estimate uncertainties in the time-averaged velocity components and turbulence intensities that varied from 1–3% (Lee 2006).

Three different sizes of sediments were used for this study. The properties of the sediment are listed in Table 1. The size distribution is characterized by d_{50} and the geometric standard deviation of the distribution, $\sigma_g = (d_{84}/d_{16})^{1/2}$. All bed materials used for this study can be considered to be uniform in size since $\sigma_g < 1.5$.

Several different sizes and shapes of bridge piers were fabricated for this study corresponding to the prototype bridge piers supporting three different river bridges in Georgia as shown in the data summary in Table 2. Model scales varied from 1:23–1:90, and the model pier widths ranged between 2.1–5.5 cm (Sturm et al. 2004). Flat-bed models refer to models of a single pier bent placed in a rectangular flume, while river models were constructed with complete geometric similarity of the river cross sections and the bridge including abutments and all pier bents.

Table 1. Characteristics of Sediments for This Study

Sediment	d_{50} (mm)	σ_g	d_*	Shields (τ_{*c})	u_{*c} (m/s)
A	3.30	1.30	83.5	0.045	0.049
B	1.10	1.33	27.8	0.038	0.026
C	0.53	1.17	13.4	0.032	0.017

The bridge approach section was located at a distance of $10b$ upstream of a bridge pier in the streamwise direction. The approach flow for each experiment was a fully-developed turbulent open channel flow in both the horizontal and tilting flumes. The approach flow velocity V_1 and shear velocity u_{*1} were obtained from a velocity profile at the approach section with point velocities measured from near the bed to a position located at 60% of the depth above the bed and fitted by the logarithmic velocity distribution. Keulegan's equation for mean velocity in turbulent flow was chosen to evaluate the critical velocities for initiation of motion of sediment in the field and laboratory using an equivalent sand-grain roughness of $k_s=2d_{50}$ and the critical value of the

Table 2. Summary of Measured Experimental Data for This Study (Chattahoochee R. Model: Runs 1–21; Flint R. Model: Runs 22–34; and Ocmulgee R. Model: Runs 35–38)

Run	Model type/scale	Q (m^3/s)	d_{50} (mm)	b (m)	y_1 (m)	V_1 (m/s)	T (hrs)	d_s (m)	V_1/V_c	y_1/b	b/d_{50}	d_s/b	Sh
1	FB/1:23.3	0.196	3.30	0.0458	0.166	0.447	24	0.056	0.64	3.62	13.9	1.22	R
2	FB/1:23.3	0.238	3.30	0.0458	0.191	0.504	32	0.081	0.70	4.17	13.9	1.77	R
3	FB/1:23.3	0.238	3.30	0.0458	0.171	0.523	36	0.100	0.74	3.73	13.9	2.18	R
4	FB/1:23.3	0.273	3.30	0.0458	0.191	0.547	36	0.103	0.76	4.17	13.9	2.25	R
5	FB/1:23.3	0.238	3.30	0.0458	0.180	0.554	36	0.121	0.78	3.93	13.9	2.64	R
6	FB/1:23.3	0.238	3.30	0.0458	0.157	0.575	36	0.128	0.83	3.43	13.9	2.79	R
7	FB/1:23.3	0.289	3.30	0.0458	0.191	0.600	36	0.134	0.83	4.17	13.9	2.92	R
8	FB/1:23.3	0.238	3.30	0.0458	0.153	0.626	38	0.134	0.91	3.34	13.9	2.92	R
9	FB/1:23.3	0.289	3.30	0.0458	0.153	0.738	37	0.135	1.07	3.34	13.9	2.95	R
10	FB/1:40	0.030	0.53	0.0270	0.107	0.260	28	0.070	0.90	3.96	50.9	2.59	R
11	FB/1:23.3	0.051	0.53	0.0458	0.191	0.257	30	0.093	0.82	4.17	86.4	2.03	R
12	FB/1:23.3	0.044	0.53	0.0458	0.142	0.304	12	0.090	1.01	3.10	86.4	1.96	R
13	RM/1:40	0.127	3.30	0.0270	0.191	0.546	48	0.062	0.76	7.07	8.2	2.30	R
14	RM/1:40	0.142	3.30	0.0270	0.191	0.588	48	0.063	0.82	7.07	8.2	2.33	R
15	RM/1:40	0.069	3.30	0.0270	0.109	0.532	48	0.080	0.82	4.04	8.2	2.96	R
16	RM/1:40	0.068	3.30	0.0270	0.109	0.546	48	0.088	0.84	4.04	8.2	3.26	R
17	RM/1:40	0.071	1.10	0.0270	0.190	0.317	48	0.060	0.71	7.04	24.5	2.22	R
18	RM/1:40	0.038	1.10	0.0270	0.107	0.308	47	0.052	0.75	3.96	24.5	1.93	R
19	RM/1:40	0.085	1.10	0.0270	0.190	0.348	47	0.059	0.78	7.04	24.5	2.19	R
20	RM/1:40	0.042	1.10	0.0270	0.107	0.341	47	0.060	0.83	3.96	24.5	2.22	R
21	RM/1:40	0.047	1.10	0.0270	0.107	0.411	47	0.068	1.00	3.96	24.5	2.52	R
22	FB/1:50	0.219	3.30	0.0366	0.160	0.486	48	0.038	0.70	4.37	11.1	1.04	R
23	FB/1:50	0.218	3.30	0.0366	0.152	0.520	48	0.050	0.75	4.16	11.1	1.37	R
24	FB/1:50	0.251	3.30	0.0366	0.158	0.537	48	0.053	0.77	4.32	11.1	1.45	R
25	FB/1:50	0.283	3.30	0.0366	0.165	0.559	48	0.084	0.88	4.51	11.1	2.30	R
26	FB/1:90	0.026	0.53	0.0203	0.128	0.189	143	0.032	0.64	6.30	38.3	1.57	R
27	FB/1:90	0.033	0.53	0.0203	0.128	0.237	24	0.041	0.80	6.30	38.3	2.02	R
28	FB/1:50	0.042	0.53	0.0366	0.149	0.263	28	0.072	0.87	4.07	69.0	1.97	R
29	FB/1:50	0.079	0.53	0.0366	0.226	0.342	12	0.066	1.07	6.18	69.0	1.80	R
30	FB/1:33	0.054	0.53	0.0554	0.241	0.215	48	0.046	0.67	4.35	105	0.83	R
31	FB/1:33	0.052	0.53	0.0554	0.170	0.281	24	0.085	0.91	3.07	105	1.53	R
32	RM/1:90	0.042	1.10	0.0203	0.152	0.247	48	0.022	0.57	7.48	18.5	1.08	R
33	RM/1:90	0.047	1.10	0.0203	0.152	0.290	96	0.037	0.67	7.48	18.5	1.82	R
34	RM/1:90	0.051	1.10	0.0203	0.152	0.335	96	0.058	0.78	7.48	18.5	2.85	R
35	FB/1:45	0.061	0.53	0.0406	0.183	0.333	10	0.082	1.07	4.50	76.7	2.01	C
36	RM/1:45	0.136	1.10	0.0406	0.181	0.312	98	0.083	0.71	4.45	36.9	2.05	C
37	RM/1:45	0.165	1.10	0.0406	0.191	0.336	92	0.089	0.75	4.70	36.9	2.20	C
38	RM/1:45	0.184	1.10	0.0406	0.203	0.350	92	0.084	0.78	5.00	36.9	2.06	C

Note: Model type: FB=flat bed; RM=river model. Sh=pier shape: R=rectangular; and C=circular.

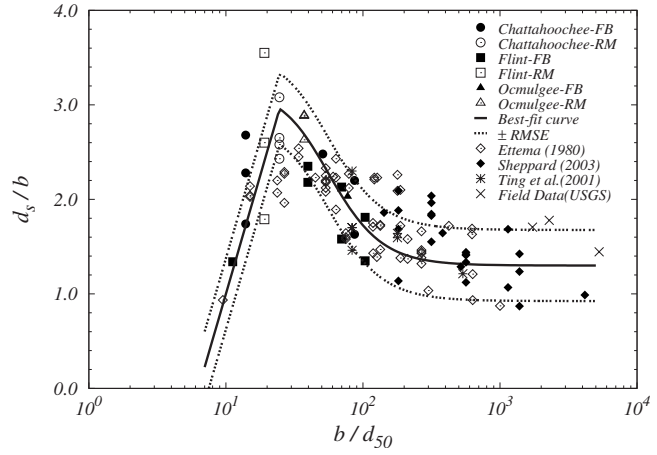

Fig. 1. Effect of b/d_{50} on the corrected d_s/b for $F_1 < 0.4$

shear velocity from Shields' diagram. As shown in Table 2, values of V_1/V_c varied from 0.6–1.0 so that the experiments were in the clear-water scour regime. Equilibrium scour depth, d_s, was determined by plotting the ADV distance to the bed as a function of the logarithm of time and continuing the experiment for at least 3 h after the bed elevation measurements showed negligible changes with time. The empirical formula of Melville and Chiew (1999) for equilibrium scour time was used as a guide in this regard. Time to equilibrium was typically 2–4 days.

In addition to detailed measurements of the approach velocity profile upstream of the pier, time records of instantaneous velocities were measured just upstream of the pier and near the bed. These measurements were taken at the beginning of scour to investigate further the scouring mechanism as related to observed oscillations in the horseshoe vortex system.

In the following sections, results for scour depth as a function of b/d_{50} are presented and discussed, and then the unsteady characteristics of the horseshoe vortex system are investigated to suggest that b/d_{50} reflects the ratio of a sediment transport time scale to a turbulent particle lifting time scale, both of which arise from the coherent structure of the horseshoe vortex system.

Effect of Sediment Size Scaling on Scour Depth Results

The ratio of pier width to sediment size, b/d_{50}, is strongly implicated in the lack of agreement between field measurements of pier scour and predictions of pier scour based on formulas derived from laboratory data. Recent literature shows that d_s/b depends on the effect of b/d_{50} at large scales (Sheppard et al. 2004; Sheppard and Miller 2006) as well as at smaller laboratory scales. In general, smaller values of b/d_{50} can impede the scour process effectively and confine the development of scour depth and width. This effect has been attributed to the dissipating effect of the pores of the larger sediment on the downflow of the horseshoe vortex (Melville and Coleman 2000). What is less clear is why d_s/b should also decrease at very large values of b/d_{50} (Sheppard et al. 2004). This study presents the development of a more comprehensive relationship between d_s/b and b/d_{50} in a way that unifies both experimental and field data, and relates it to the general large-scale unsteady flow characteristics of the horseshoe vortex system.

The experimental data in this study are plotted along with field measurements from the three field sites monitored by the USGS in a field and laboratory study of bridge scour (Sturm et al. 2004) in Fig. 1 in which all values of d_s/b were corrected with several factors related to the effects of flow intensity, pier shape, flow depth, and skewness due to the angle of attack presented by Melville and Sutherland (1988) so as to isolate the effects of b/d_{50} on maximum pier scour depth. First, the value of d_s/b was divided by the value from the correction equation for V_1/V_c if $V_1/V_c < 1$ (clear-water scour condition), but if not, live-bed scour conditions were assumed and no correction for V_1/V_c was made based on recommendations of the Melville and Sutherland formula. The factor of pier shape was also applied as a correction. The correction factor for flow depth was considered only if $y_1/b < 2.6$ and the correction factor for pier alignment was that suggested in HEC-18 (Richardson and Davis 2001). While the Flint River pier had a shallow buried footing, the foundation geometry correction suggested by Melville and Raudkivi (1996) for this case is small within a range of large uncertainty and does not significantly change the root-mean-square error (RMSE) of the overall regression fit, so it was not included.

From an analysis of the complete data set from this study as well as data by others, it was determined that the data segregate according to a value of the approach flow Froude number, $F_1 \cong 0.4$. Although the case of $F_1 > 0.4$ with $b/d_{50} < 20$ was investigated, it is not discussed further herein because it is a less common condition. The data in Fig. 1 are restricted to cases of $F_1 < 0.4$ for which the bow wave just upstream of the pier is relatively small.

In Fig. 1, there is clearly a peak where the value of $b/d_{50} \cong 25$ when the corrected values of d_s/b from the laboratory data of this study are plotted with respect to b/d_{50}. This is in accord with the critical values presented in the literature (Breusers and Raudkivi 1991; Hoffmans and Verheij 1997; Melville 1997). However, these investigators suggest that no effect of b/d_{50} needs to be considered if $b/d_{50} > 25$; in other words, they assume that no correction factor for b/d_{50} is necessary in this upper range (Melville and Coleman 2000).

Laboratory data from the literature have been added to Fig. 1 in order to show more detailed trends and a wider range of applicability. Using a more extensive data set from the literature (Ettema 1980; Sheppard 2003; Sheppard et al. 2004; Sheppard and Miller 2006; Ting et al. 2001), the correction factors proposed by Melville and Sutherland (1988) were also applied to the expanded data set to maintain consistency in isolating the effect of b/d_{50}. Most experimental data in the range of $b/d_{50} = 140-4160$ are from the clear-water scour experiments of Sheppard (2004) in a 6.1 m wide, 6.4 m deep, and 38.4 m long flume at the USGS Conte Research Center in Turners Falls, Massachusetts. Also, the field data measured by the USGS in this study for the Chattahoochee, Flint, and Ocmulgee Rivers in Georgia have been included in Fig. 1. The full data set in Fig. 1 indicates a decrease in d_s/b as b/d_{50} increases beyond 25.

A least-squares regression analysis was applied to the data in which the data were divided into two groups by the criterion of $b/d_{50} > 25$ or $b/d_{50} < 25$. The resulting relationships shown in Fig. 1 between d_s/b and b/d_{50} are

$$\frac{d_s}{b} = 5.0 \log\left(\frac{b}{d_{50}}\right) - 4.0, \quad 6 \leq b/d_{50} \leq 25 \tag{2a}$$

$$\frac{d_s}{b} = \frac{1.8}{(0.02b/d_{50} - 0.2)^2 + 1} + 1.3, \quad 25 \leq b/d_{50} \leq 1 \times 10^4 \tag{2b}$$

For $b/d_{50} \leq 25$, d_s/b increases logarithmically with b/d_{50}, while it decreases for $b/d_{50} > 25$. For $b/d_{50} > 400$, $d_s/b \approx 1.3$. Also shown

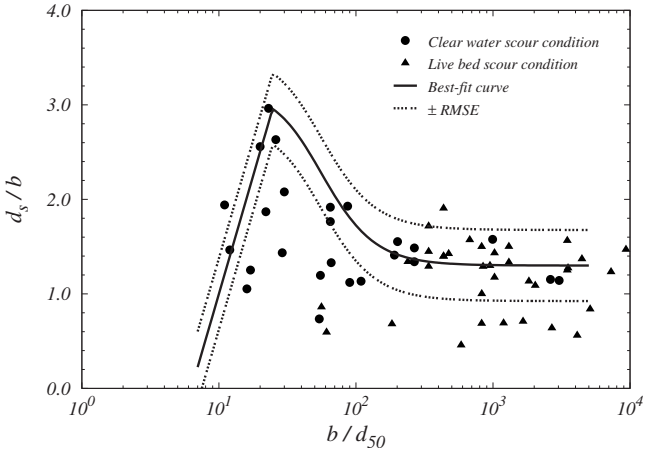

Fig. 2. Corrected relative scour depth, d_s/b, as a function of b/d_{50} for selected field data with $F_1<0.4$ (Mueller and Wagner 2005)

in Fig. 1 are confidence limits in $d_s/b=\pm 1\times$RMSE for the entire data set for which RMSE=0.38. While the trend for smaller values of b/d_{50} is similar to that reported by several other investigators, the case of $b/d_{50}>25$ is of particular interest in this study, and will be discussed in more detail subsequently.

Using the field measurements of Landers and Mueller (1996) and Mueller and Wagner (2005), the applicability of Eq. (2) to field data are examined in Fig. 2. Before comparing the field data with the laboratory-derived equations, the field data were filtered from 493 local pier scour measurements presented by Mueller and Wagner (2005), many of which were reported earlier by Landers and Mueller (1996). In the latter report, no relationship was found between d_s/b and b/d_{50} when using the full data set. First, data were selected only for $F_1<0.4$, and second, data affected by debris accumulation on the pier were eliminated. Third, data points were deleted if $d_{50}<0.1$ mm, so as not to consider cohesive sediment effects. Fourthly, in the cases for which pier scour depths were measured both upstream and downstream of the bridge, only the maximum value of scour depth was selected. Finally, in cases where scour monitoring over time was conducted at the same bridge pier, only the maximum recorded scour depth was selected and presented in Fig. 2. This left a total of 66 field data points, 26 of which were for clear-water scour conditions and 40 of which represented live-bed scour conditions. The filtered data are plotted in Fig. 2 along with the laboratory-derived curve from Fig. 1.

For clear-water scour conditions, most of the field data in Fig. 2 show reasonable agreement with the laboratory derived curve. In fact, the upper confidence limit curve serves as a reasonable upper envelope of the filtered field data in both clear-water and live-bed regimes. For those clear-water scour data points plotting significantly below the curve, it can be argued that the scour depths had not reached the equilibrium or maximum state at the time of measurement because of the short duration of the flood relative to equilibrium time. Considerable uncertainty occurs for this method of field scour measurement because it is never known whether the bed has reached an equilibrium state at the time of scour and discharge measurements. Similar discrepancies occurred for the live-bed scour data but perhaps for different reasons. Even though the measured scour depth may represent equilibrium scour conditions for live-bed scour, it is possible that the measured scour depths were sometimes less and sometimes more than the equilibrium value due to dynamic flow characteristics and sediment transport conditions in the field such as the passage of dunes through the scour hole. However, overlaying the best-fit laboratory curve on top of the filtered field data as shown in Fig. 2 provides confirmation of the decrease and leveling off of d_s/b values as b/d_{50} increases from 25 to the large values often observed in the field. In the next section, we engage the question of why b/d_{50} should affect scour depths in terms of the large-scale unsteady characteristics of the horseshoe vortex system.

Scaling of Large-Scale Unsteadiness of Horseshoe Vortex System

In general, the local flow structure around a bridge pier consists of flow separation as the pier obstacle is approached, the downflow at the upstream face of the pier in the vertical plane, the horseshoe vortex system that wraps around the base of the pier, the bow wave near the free surface on the upstream face of the pier, and the wake vortex system at the rear of the bridge pier that extends over the flow depth. The horseshoe vortex system upstream of a bridge pier is perhaps the most evident and significant contributor to the scour process. Previous studies have focused on measuring the turbulence in the horseshoe vortex system as a stationary process (Unger and Hager 2007; Dey and Raikar 2007; Graf and Istiarto 2002; Melville and Raudkivi 1977), at least with respect to a specific phase of the long-term scour hole development with time. However, Dargahi (1989) has described experimental observations of the formation of multiple secondary vortices in the horseshoe vortex system that oscillate irregularly as they combine and stretch around the pier and then pull back into the primary vortex again on a time scale of the order of $10b/V_1$. Most methods presented in the literature for describing the horseshoe vortex properties have not considered the effect of these coherent turbulent motions on pier scour or how they should be scaled in the laboratory.

In the following sections, the coherent structure of the horseshoe vortex is made evident using the tools of flow visualization, velocity probability distributions, and phase averaging. Phase averaging is introduced to isolate the quasiperiodic components of the velocity and to identify the time scales of the coherent motion that are thought to be relevant to the observed variation of scour depth with b/d_{50} that was presented and discussed in the previous section.

Observations of Sediment Movement

From a preliminary flow visualization in front of a pier, it became apparent that the primary horseshoe vortex oscillates in position and size over a time scale that is large with respect to the turbulence time scale associated with the largest eddies in the approach flow. This temporal variation of the horseshoe vortex upstream of a bridge pier would account for variability in the direction of instantaneous velocities near the bed as the horseshoe vortex and the point of flow separation oscillate back and forth in the streamwise direction. It is suggested in this paper that sediment grains in front of a bridge pier move irregularly in space and time due to the large-scale unsteadiness of the horseshoe vortex even if the approach flow is steady.

To further investigate the motion of sediment near the pier, a video camera was used to record the motion of sediment particles in front of a pier. Two different sizes of sediments, $d_{50}=0.5$ mm and 3.3 mm, were chosen to examine the features of the unsteady, large-scale coherent sediment motions in the horseshoe vortex system as affected by two different values of b/d_{50} for the same

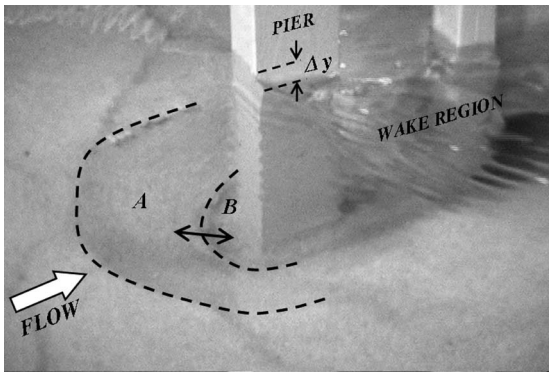

Fig. 3. Motion of sediment grains for $V_1/V_c=0.70$, $y_1/b=5.0$, $b/d_{50}=50.9$ [(A) outer slope; (B) inner slope; and Δy=bow wave height]

values of V_1/V_c and y_1/b. The sequence of images for each case was captured by focusing on the region in front of the bridge pier as shown in Figs. 3 and 4.

For the finer sediment case ($b/d_{50}=50.9$) in Fig. 3, there are two different slopes of the scour hole in front of the pier. The outer slope is approximately equal to the angle of repose of the sediment while the inner slope underneath the primary horseshoe vortex is steeper than that of the outer one because this portion is affected by the combination of the downflow at the pier and rotation of the horseshoe vortex. The boundary between the outer and inner slope oscillated in position as the horseshoe vortex expanded and contracted as shown schematically by the arrows in Fig. 3. A marked suspended sediment particle was observed in a sequence of frames over a total duration of approximately $26b/V_1$. First, the particle slid into the inner scour hole as the edge of the outer slope collapsed. Then, the particle moved back to the upstream boundary of the inner scour hole due to the irregular oscillation of the horseshoe vortex while it remained suspended and at the same time, the particle drifted transversely along the pier following the limbs of the horseshoe vortex. Finally, it fell into the inner scour hole again due to the slope failure of the outer slope and was washed out as the horseshoe vortex contracted and its limbs wrapped around the pier.

For the coarser sediment ($b/d_{50}=8.2$), the motion of the sediment particles (Fig. 4) differs from that at the higher value of b/d_{50} (Fig. 3). There is no evident reverse motion and suspension due to the horseshoe vortex but rather motion similar to bedload

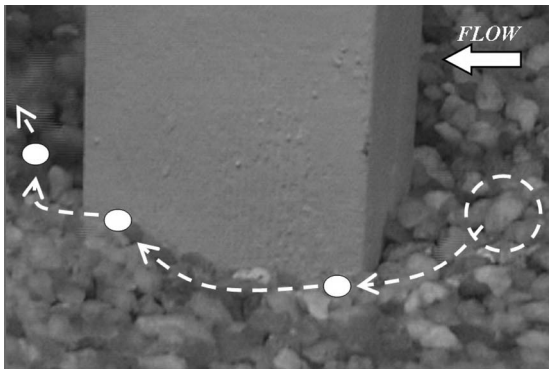

Fig. 4. Motion of sediment grains for $V_1/V_c=0.70$, $y_1/b=5.0$, and $b/d_{50}=8.2$

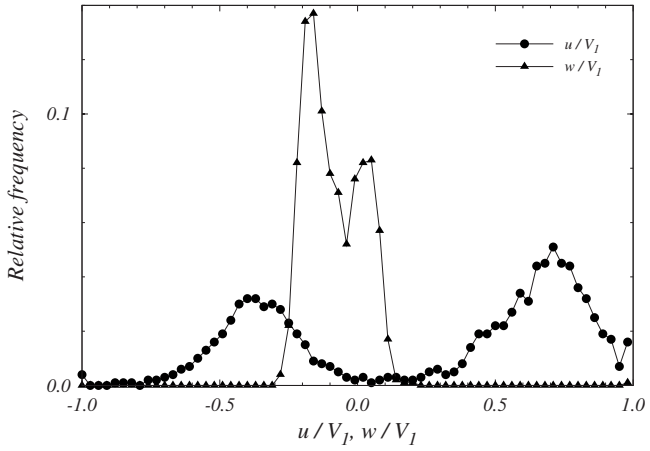

Fig. 5. Velocity probability distributions from experimental run 7 at $x/b=-0.33$, $z/b=0.17$, and $z/y_1=0.04$ (V_1=approach velocity)

transport in a river. The particle marked with the dashed circle vibrates apparently in response to turbulence fluctuations and then moves in a short sliding step only to come to rest again. The particle motion continues as a series of short steps until it is washed out along the pier by the contracting limb of the horseshoe vortex over a total time period of approximately $30b/V_1$.

Bimodal Probability Distribution of Velocity

The instantaneous velocity time series when measured near the bed at a particular point in front of the pier alternately exhibited periods of positive streamwise velocity toward the pier followed by negative streamwise velocity away from the bridge pier. This horizontal location was at $x/b=-0.33$, where x=streamwise coordinate positive in the flow direction and zero at the upstream face of the pier, and it corresponds approximately to the primary separation point of the horseshoe vortex system reported by Dargahi (1989) for a single cylinder. The result is a bimodal probability distribution of velocity as shown in Fig. 5 and described by Devenport and Simpson (1990) for a wing/flat-bed junction studied in a wind tunnel. They suggested that the two alternate states of the horseshoe vortex (expanded and contracted) are bistable, with the contracted mode occurring about 20–30% of the time. They further hypothesized that the large-scale unsteadiness is caused by the intermittent turbulent structure of the fluid in the outer portion of the boundary layer being drawn into the corner formed by the wing and lower solid boundary. In their numerical simulation of the horseshoe vortex in front of a bridge pier, Kirkil et al. (2008) likewise observed this behavior and attributed it to an intermittent wall-attached jet resulting from entrainment of patches of high-momentum low-vorticity fluid in the downflow from the outer part of the boundary layer.

A bimodal probability distribution with dual peaks was observed in this study for both the streamwise and vertical velocity components at a selected measuring location on a fixed flat bed for experimental run 7 as shown in Fig. 5 for $x/b=-0.33$ and $z/b=0.17$, where x=streamwise coordinate positive in the flow direction and zero at the upstream face of the pier; and z=vertical coordinate positive upward with zero at the initial bed elevation. A thin layer of reverse flow exists near the bed due to the horseshoe vortex which accounts for the negative streamwise velocity, but as the separation point retreats to a position closer to the pier, the streamwise velocity becomes positive at the measur-

ing location, resulting in a bimodal probability distribution. For this particular measuring location, positive values of the vertical velocity component are consistent with the reverse streamwise velocity as the primary vortex expands while negative values of the vertical velocity component are likely associated with a secondary vortex upstream of the primary vortex as the primary vortex contracts toward the pier as visualized by Dargahi (1989). For higher values of z/b above the bed, the bimodal feature of the probability distribution was not observed to occur. Devenport and Simpson (1990) found that the shape, relative size, and distance between the two peaks of the bimodal probability density function are not permanent and stable, but instead vary with the vertical position of the velocity measurement. The velocity measurements shown in Fig. 5 for one particular location near the region of flow separation clearly demonstrate the unsteady oscillation of the primary horseshoe vortex between two modes.

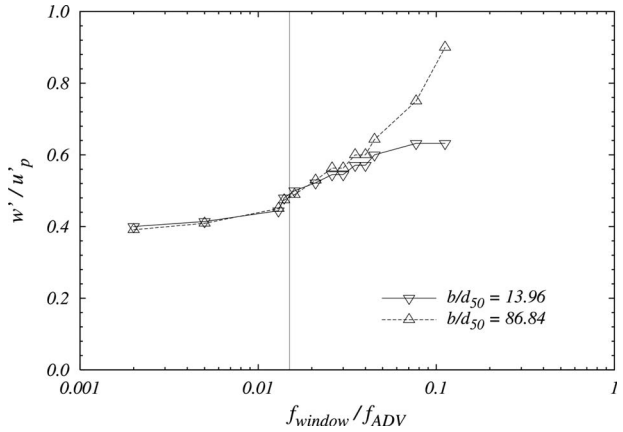

Fig. 6. Ratio of the vertical turbulence intensity to root mean square value of u_p in streamwise direction after phase averaging

Coupling between Scaling of Large-Scale Unsteadiness and b/d_{50}

As observed by Nelson et al. (1995), sediment transport rates in nonuniform flows, such as the wake region downstream of a backward-facing step, are related to the frequency structure of coherent turbulent events. Chrisohoides et al. (2003) studied coherent turbulent structures in flat-bed abutment flows and suggested that sediment transport relationships in this complex 3D flow must consider the structure of the large-scale foundation-induced vortices. Similarly, the horseshoe vortex in front of a bridge pier produces large-magnitude, low-frequency events associated with the quasiperiodic unsteadiness of its location and shape that may contribute significantly to the scour process.

In order to further investigate the coupling between the large-scale unsteadiness of the horseshoe vortex and b/d_{50}, it is hypothesized that the scour process occurs in two steps: first, sediment is detached from the bed and then it is entrained into the flow to be transported downstream as observed in the videos of sediment movement described previously. The sediment grains slide, roll, and jump periodically from the bed due to the frequency of the vertical turbulent fluctuations that act to lift the sediment off the bed, while all or a portion of the dislodged grains are transported downstream out of the scour hole at a streamwise frequency associated with the frequency of oscillation of the horseshoe vortex. What is required, therefore, is to extract the unsteady or frequency characteristics of the coherent structure of the horseshoe vortex from the velocity time series.

Based on the results of observations of sediment movement and probability analysis, phase-averaging is introduced to investigate in more detail the periodic time scale in the time series associated with the intermittency of the primary horseshoe vortex size as the separation point oscillates between two preferred states in the streamwise direction. This method is implemented by averaging the instantaneous velocity over an appropriate measuring period or window size for a long time series. The size or magnitude of the window should be chosen to distinguish between the periodic variations and the residual turbulent fluctuations (Zhang et al. 1997). In the general unsteady-in-the-mean turbulent flow, the instantaneous velocity, $u(t)$, can be decomposed into three components: $u(t)=U+\hat{u}(t)+u''(t)=u_p(t)+u''(t)$, where U=global mean velocity over a long time period; $\hat{u}(t)$ =statistical contribution of the organized periodic component; $u''(t)$=instantaneous value of velocity fluctuations (turbulence); and $u_p(t)$=phase-averaged velocity.

The velocity time series was measured at a single point located at $x/b=-0.3$ upstream of the pier and at a relative elevation of $z/b=0.17$ (or $z/y_1=0.04$) over a duration of 5 min for experimental runs 7 and 11 in Table 2 having values of b/d_{50} of 13.9 and 86.4, respectively, but the same values of V_1/V_c and y_1/b. Observation of the time series of the streamwise velocity components suggested that filtering was needed to distinguish the irregular periodic motion. The time series of velocity measurements was filtered with a Gaussian low-pass filter having a cutoff frequency of 1.25 Hz before applying the phase-averaging technique. Through Gaussian filtering of the high frequency fluctuations and electronic noise, the periodic velocity components of a certain frequency can be identified. Power spectral analysis of the filtered streamwise velocity signal revealed a significant peak at 0.25 Hz for experimental run 7 and 0.32 Hz for run 11 which further suggested the existence of a periodic component associated with the coherent structure and justified the use of phase analysis to separate it out. These frequencies correspond to Strouhal numbers of the horseshoe vortex, $\mathsf{S}=fb/V_1=0.02$ and 0.06, respectively, which are comparable to the value of 0.05 observed by Devenport and Simpson (1990) for a wing-body junction with an elliptical nose at the same order of R_b. Dargahi (1989) reported a wide range of $\mathsf{S}=0.06$ to 1.0 corresponding to shedding frequencies of different vortices in the horseshoe vortex system upstream of a cylinder in a flume flow at a similar value of R_b.

The vertical mobilization of sediment in front of the pier is assumed related to the total fluctuation of the vertical velocity component w' with respect to the global time average. On the other hand, the frequency of the sweeping of dislodged sediment out of the scour hole is thought to be dependent on the *rms* fluctuation in the phase-averaged streamwise periodic component of velocity, u'_p, measured at the nose of the pier. Fig. 6 is a plot of the ratio of these velocity scales, w'/u'_p, versus the relative frequency ratio, $f_{\text{window}}/f_{\text{ADV}}$, which is the ratio of the frequency associated with the window size for phase averaging to the sampling frequency of the ADV (25 Hz). As shown in Fig. 6, the appropriate window size for identifying the periodic component occurs for $f_{\text{window}}/f_{\text{ADV}}<0.02$ as w'/u'_p levels off to a constant value of approximately 0.4. This constant value is essentially the same for both runs 7 and 11 which have very different values of b/d_{50} but the same values of y_1/b and V_1/V_c.

Based on the constant value of w'/u'_p, the bimodal characteristics of the horseshoe vortex, and the visualization of sediment movement, two time scales governing the scour process are proposed. One is the time for lifting or dislodging sediment particles

to mobilize or entrain them, and the other is the time for sweeping or transporting the sediment particles out of the scour hole. Both time scales can be represented as a function of sediment size, pier width, and the velocity scales identified in Fig. 6 as follows:

$$t_L \sim \frac{\alpha_L d_{50}}{w'} \tag{3}$$

$$t_T \sim \frac{\alpha_T b}{u_p'} \tag{4}$$

where t_L=time scale for lifting or mobilizing sediment particles; t_T=time scale for transporting particles out of the scour hole; and α_L and α_T=coefficients of proportionality. The value of α_L defines the grain lifting height in terms of the number of grain diameters. This is analogous to the grain movement step size in Einstein's sediment bedload formulation (Sturm 2001), or perhaps more appropriately to the saltation (jumping or hopping) height in the bedload equation of van Rijn (1984). The value of α_T reflects the distance relative to the pier diameter to be traveled by a mobilized sediment grain from the scour hole in front of the pier to the wake zone.

The relationship between t_L and t_T can be defined in terms of b/d_{50} assuming that the ratio, w'/u_p', is a constant equal to 0.4 (Fig. 6) for the same values of y_1/b and V_1/V_c but different values of b/d_{50}. The ratio of the two time scales is

$$\frac{t_T}{t_L} = \frac{\alpha_T b}{\alpha_L d_{50}} \times \frac{w'}{u_p'} = \frac{1}{25} \times \frac{b}{d_{50}} \tag{5}$$

in which it has been assumed for the sake of argument, that the average height of grain suspension is of the order of ten grain diameters, i.e., $a_L \approx 10$ (van Rijn 1984), while $a_T \approx 1$. For these assumptions, the pier scour depth maximum that occurs when $b/d_{50} \approx 25$ corresponds to $t_T/t_L \approx 1.0$. Equivalently, the maximum equilibrium pier scour depth occurs when the frequency of suspension or lifting events due to turbulence, f_L, is matched to the frequency of transport events, f_T, caused by pulsation of the horseshoe vortex; that is, $t_T/t_L = f_L/f_T \approx 1.0$.

Eq. (5) reflects the effects of both the turbulence characteristics and unsteadiness of the horseshoe vortex system associated with the coherent structure. Three categories in terms of the frequencies, f_L and f_T, can be defined to explain the effect of b/d_{50} on d_s/b. First, the maximum d_s/b occurs when $f_L \approx f_T$ at $b/d_{50} \approx 25$. When $f_L > f_T$ for $b/d_{50} > 25$, d_s/b decreases with increasing values of b/d_{50} which corresponds to the large scale pier diameter in the field relative to sediment grain size. The entire bed in front of the bridge pier periodically becomes fluidized and suspended due to the action of w', but the greater frequency of the suspension events compared to the frequency of the entrainment and transport events due to the horseshoe vortex means that not all of the available sediment can be carried out of the scour hole so that some of it is redeposited. In effect, there is insufficient transport capacity relative to the available suspended sediment. The net result is a reduction in the maximum scour depth at the nose of the bridge pier as the scale becomes larger. For $f_L < f_T (b/d_{50} < 25)$, d_s/b also decreases but with decreasing values of b/d_{50} since the frequency of suspension events is too small for the available transport capacity attributed to the frequency of oscillation in the horseshoe vortex. In this case, the scour process becomes suspension limited. This explanation of the effect of b/d_{50} on d_s/b assumes similarity of w'/u_p' at small and large scales, at least up to a point. It seems to be consistent both with the observations of Ettema et al. (2006) and of Sheppard et al. (2004). The higher frequencies of vortex shedding at small scales compared to large scales results in more scour because of the scale distortion caused by a smaller value of b/d_{50} in the laboratory than in the field. It must be noted, however, that the frequency scaling argument of Ettema et al. (2006) was applied to the wake vortices rather than the horseshoe vortex.

For $b/d_{50} > 400$, further decreases in scour depth become small. At very large turbulent scales, the coherent structure may change such that w'/u_p' is no longer constant but rather decreases such that distortion in scaling of scour becomes irrelevant. Hence, the approach of the normalized d_s/b to a relatively constant value for $b/d_{50} > 400$ may reflect a Reynolds number effect in the sense that if the Reynolds number is large enough, the frequency ratio of sediment lifting to transport is no longer changing. However, more extensive measurements of coherent structure at large values of the Reynolds number are needed.

Conclusions

The contribution of this study to the problem of bridge pier scour prediction lies primarily in the investigation of the scaling effect of relative sediment size on laboratory values of pier scour depth and its relationship to the coherent structure of the horseshoe vortex. Extensive laboratory model tests of three different prototype bridge piers with three different sediment sizes were conducted using flat-bed models of individual bridge pier bents as well as full hydraulic river models of the river bathymetry, bridge piers, and abutments at different geometric scales. From analysis of data in this study as well as from other laboratory and field studies reported in the literature, it was found that the relative scour depth is a unique function of the ratio of pier width to sediment size, b/d_{50}, if attention is restricted to data for which the approach flow Froude number is less than 0.4. Applying regression analysis to all the laboratory data plus three field data points from this study, two continuous best-fit equations for adjusted pier scour depth as a function of b/d_{50} were developed according to the value of b/d_{50} ($\leqslant 25$ and >25). The maximum value of relative pier scour depth occurred at a value of $b/d_{50} \approx 25$ as reported by other investigators. For large values of b/d_{50}, the relative scour depth decreased in agreement with experiments in very large flumes as well as with the three field data points from this study. When compared with an independent, filtered field data set, the upper confidence limit of $1 \times$RMSE for the best-fit equations reasonably described an upper envelope for the field data.

The choice of sediment size in the laboratory model distorts the value of b/d_{50} in comparison with the prototype which in turn causes larger values of scour depth in the laboratory than in the field. This behavior was explained by the scaling, or distortion, of the large-scale unsteadiness of the horseshoe vortex which is directly related to the distortion in b/d_{50}. Time records of instantaneous velocities near the nose of the pier were taken to show that the pier scouring mechanism is related to the large-scale unsteadiness of the primary horseshoe vortex as investigated through observations of sediment movement, velocity probability distributions, and phase averaging. It was suggested that the quasiperiodic oscillation of the horseshoe vortex is related to transport of sediment particles during the scouring process. Two distinct types of sediment motion were observed for two different sediment sizes that ultimately affect the equilibrium scour depth in front of the pier. Based on phase-averaging of a long time series of velocity data in front of the pier near the oscillating point of separation caused by the large-scale unsteadiness of the horse-

shoe vortex, it was found that the ratio of the vertical turbulence intensity to the *rms* value of the phase-averaged streamwise velocity was a constant. By postulating that these two measures of turbulence velocity scales are related to the two time scales of lifting and transport of sediment particles, respectively, it was concluded that the time-scale ratio (or frequency ratio) is essentially reflected by the value of b/d_{50}. Such an explanation is consistent with smaller observed values of relative scour depth for larger field values of b/d_{50}. Further research is needed on the coherent structure of the horseshoe vortex at very large scales.

Acknowledgments

This study was supported by a grant from the Georgia Department of Transportation (GDOT).

Notation

The following symbols are used in this paper:

b = width of a bridge pier;
d_{50} = median sediment diameter for which 50% of the particles are finer by weight;
d_s = scour depth;
d_* = dimensionless sediment diameter $=[(\gamma_s/\gamma-1)gd_{50}^3/\nu^2]^{1/3}$;
F_b = pier Froude number, $=V_1/\sqrt{gb}$;
F_1 = Froude number of approach flow, $=V_1/\sqrt{gy_1}$;
f_L = frequency of lifting or mobilization of sediment grains due to w';
f_T = frequency of transport of sediment grains out of scour hole; by quasiperiodic fluctuation in horseshoe vortex as reflected by u_p';
f_{window} = window size in phase averaging of ADV velocity signal;
f_{ADV} = sampling frequency of ADV;
g = acceleration due to gravity;
K_s = pier shape factor;
K_θ = pier skewness factor;
k_s = equivalent sand grain roughness height;
Q = flowrate;
R_b = pier Reynolds number, $=V_1b/\nu$;
R_1 = approach flow Reynolds number, $=V_1y_1/\nu$;
S = Strouhal number associated with frequency of horseshoe vortex oscillation$=fb/V_1$;
T = duration of scour experiment;
t_L = time scale of lifting or mobilization of sediment grains;
t_T = time scale of entrainment and transport of sediment grains out of scour hole;
U = global mean velocity over a long time period;
u,v,w = instantaneous velocity components in x, y, and z directions;
u',v',w' = turbulent velocity fluctuations in x, y, and z directions;
$u''(t)$ = instantaneous value of turbulent fluctuations in phase-averaged signal;
$\hat{u}(t)$ = statistical contribution of the organized periodic component;
u_p = phase-averaged velocity of coherent structure;
u_p' = *rms* fluctuation of phase-averaged velocity;
u_* = shear velocity;
u_{*c} = critical shear velocity$=(\tau_c/\rho)^{1/2}$;
V_1 = depth-averaged velocity of approach flow;
V_c = critical flow velocity corresponding to initiation of sediment motion;
x,y,z = streamwise, cross-stream, and vertical coordinates, respectively;
y_1 = depth of approach flow;
α_L = coefficient of proportionality in definition of time scale t_L;
α_T = coefficient of proportionality in definition of time scale t_T;
γ = specific weight of water;
γ_s = specific weight of a sediment particle;
σ_g = geometric standard deviation of sediment size distribution;
ν = kinematic viscosity;
τ_c = critical shear stress for initiation of sediment motion; and
τ_{*c} = critical value of Shields' parameter $=\tau_c/[(\gamma_s-\gamma)d_{50}]$.

References

Breusers, H. N. C., and Raudkivi, A. J. (1991). *Scouring*, International Association for Hydraulic Research, Balkema, Rotterdam, The Netherlands.

Chrisohoides, A., Sotiropoulos, F., and Sturm, T. W. (2003). "Coherent structures in flat-bed abutment flow: Computational fluid dynamics simulations and experiments." *J. Hydraul. Eng.*, 129(3), 177–186.

Dargahi, B. (1989). "Turbulent flow field around a circular cylinder." *Exp. Fluids*, 8(1–2), 1–12.

Devenport, W. J., and Simpson, R. L. (1990). "Time-dependent and time-averaged turbulence structure near the nose of a wing-body junction." *J. Fluid Mech.*, 210, 23–55.

Dey, S., and Raikar, R. V. (2007). "Characteristics of horseshoe vortex in developing scour holes at piers." *J. Hydraul. Eng.*, 133(4), 399–413.

Ettema, R. (1980). "Scour at bridge piers." *Rep. No. 216*, Dept. of Civil Engineering, Univ. of Auckland, Auckland, New Zealand.

Ettema, R., Kirkil, G., and Muste, M. (2006). "Similitude of large-scale turbulence in experiments on local scour at cylinders." *J. Hydraul. Eng.*, 132(1), 33–40.

Ettema, R., Melville, B. W., and Barkdoll, B. (1998). "Scale effect in pier-scour experiments." *J. Hydraul. Eng.*, 124(6), 639–642.

García, C. M., Cantero, M. I., Niño, Y., and García, M. H. (2005). "Turbulence measurements with acoustic Doppler velocimeters." *J. Hydraul. Eng.*, 131(12), 1062–1073.

Ge, L., Lee, S., Sotiropoulos, F., and Sturm, T. W. (2005). "3D unsteady RANS modeling of complex hydraulic engineering flows. II: Model validation and flow physics." *J. Hydraul. Eng.*, 131(9), 809–820.

Goring, D. G., and Nikora, V. I. (2002). "Despiking acoustic Doppler velocimeter data." *J. Hydraul. Eng.*, 128(1), 117–2002.

Graf, W. H., and Istiarto, I. (2002). "Flow pattern in the scour hole around a cylinder." *J. Hydraul. Res.*, 40(1), 13–20.

Hoffmans, G. J. C. M., and Verheij, H. J. (1997). *Scour manual*, Balkema, Rotterdam, The Netherlands.

Kirkil, G., Constantinescu, S. G., and Ettema, R. (2008). "Coherent structure in the flow field around a circular cylinder with scour hole." *J. Hydraul. Eng.*, 134(5), 572–587.

Landers, M. N., and Mueller, D. S. (1996). "Evaluation of selected pier-scour equations using field data." *Transp. Res. Rec.*, 1523, 186–195.

Lee, S. O. (2006). "Physical modeling of local scour around complex bridge piers." Ph.D. thesis, Georgia Institute of Technology, Atlanta.

Melville, B. W. (1997). "Pier and abutment scour: Integrated approach." *J. Hydraul. Eng.*, 123(2), 125–136.

Melville, B. W., and Chiew, Y.-M. (1999). "Time scale for local scour at bridge piers." *J. Hydraul. Eng.*, 125(1), 59–65.
Melville, B. W., and Coleman, S. E. (2000). *Bridge scour*, Water Resources, Highlands Ranch, Colo.
Melville, B. W., and Raudkivi, A. J. (1977). "Flow characteristics in local scour at bridge piers." *J. Hydraul. Res.*, 15(4), 373–380.
Melville, B. W., and Raudkivi, A. J. (1996). "Effects of foundation geometry on bridge pier scour." *J. Hydraul. Eng.*, 122(4), 203–209.
Melville, B. W., and Sutherland, A. J. (1988). "Design method for local scour at bridge piers." *J. Hydraul. Eng.*, 114(10), 1210–1226.
Morris, J. L., and Pagan-Ortiz, J. E. (1999). "Bridge scour evaluation program in the United States." *Stream stability and scour at highway bridges*, E. V. Richardson and P. F. Lagasse, eds., ASCE, Reston, Va., 61–70.
Mueller, D. S., and Wagner, C. R. (2005). "Field observations and evaluations of streambed scour at bridges." *Report No. FHWA-RD-03–052*, U.S. Department of Transportation, Federal Highway Admin., McLean, Va.
Nelson, J. M., Shreve, R. L., McLean, S. R., and Drake, T. G. (1995). "Role of near-bed turbulence structure in bed load transport and bed form mechanics." *Water Resour. Res.*, 31(8), 2071–2086.
Parola, A. C., Hagerty, D. J., and Kamojjala, S. (1998). "Highway infrastructure damage caused by the 1993 upper Mississippi River basin flooding." *Rep. No. 417*, Transportation Research Board, Washington, D.C.
Raudkivi, A. J. (1986). "Functional trends of scour at bridge piers." *J. Hydraul. Eng.*, 112(1), 1–13.
Richardson, E. V., and Davis, S. R. (2001). "Evaluating scour at bridges." *Hydraulic Engineering Circular 18 (HEC-18)*, U.S. Federal Highway Administration, Washington, D.C.
Shen, H. W., Schneider, V. R., and Karaki, S. S. (1969). "Local scour around bridge piers." *J. Hydr. Div.*, 95(HY6), 1919–1940.
Sheppard, D. M. (2003). "Large scale and live bed local pier scour experiments." *Live bed experiments/Phase 2 Final Rep.*, Florida Dept. of Transportation.
Sheppard, D. M., and Miller, Jr., W. (2006). "Live-bed local pier scour experiments." *J. Hydraul. Eng.*, 132(7), 635–642.
Sheppard, D. M., Odeh, M., and Glasser, T. (2004). "Large scale clear-water local pier scour experiments." *J. Hydraul. Eng.*, 130(10), 957–963.
SonTek. (2001). *ADV principles of operation*, SonTek, San Diego, Calif.
Stamey, T. C. (1996). "Summary of data-collection activities and effects of flooding from Tropical Storm Alberto in parts of Georgia, Alabama, and Florida in July 1994." *Report No. 96–228*, U.S. Geological Survey, Atlanta.
Sturm, T. W. (2001). *Open-channel hydraulics*, McGraw-Hill, New York
Sturm, T. W., et al. (2004). "Laboratory and 3D numerical modeling with field monitoring of regional bridge scour in Georgia." *Georgia DOT Final Report*, Georgia Dept. of Transportation, Atlanta.
Ting, F. C. K., Briaud, J. L., Chen, H. C., Gudavalli, R., Perugu, S., and Wei, G. (2001). "Flume tests for scour in clay at circular piers." *J. Hydraul. Eng.*, 127(11), 969–978.
Unger, J., and Hager, W. H. (2007). "Down-flow and horseshoe vortex characteristics of sediment embedded bridge piers." *Exp. Fluids*, 42, 1–19.
van Rijn, L. C. (1984). "Sediment transport. I: Bed load transport." *J. Hydraul. Eng.*, 110(10), 1431–1456.
Voulgaris, G., and Trowbridge, J. H. (1998). "Evaluation of the acoustic Doppler velocimeter (ADV) for turbulence measurements." *J. Atmos. Ocean. Technol.*, 15, 272–289.
Wardhana, K., and Hadipriono, F. C. (2003). "Analysis of recent bridge failures in the United States." *J. Perform. Constr. Facil.*, 17(3), 144–150.
Zhang, Z., Eisele, K., and Hirt, F. (1997). "The influence of phase-averaging window size on the determination of turbulence quantities in unsteady turbulent flows." *Exp. Fluids*, 22(3), 265–267.